HHS Public Access

Author manuscript

J Neural Eng. Author manuscript; available in PMC 2024 January 18.

Published in final edited form as:

J Neural Eng. ; 20(1): . doi:10.1088/1741-2552/acab86.

Utah Array Characterization and Histological Analysis of a Multi-Year Implant in Non-Human Primate Motor and Sensory Cortices

Paras R. Patel[1,*], **Elissa J. Welle**[1,*], **Joseph G. Letner**[1], **Hao Shen**[1], **Autumn J. Bullard**[1], **Ciara M. Caldwell**[1], **Alexis Vega-Medina**[2,6], **Julianna M. Richie**[1], **Hope E. Thayer**[3], **Parag G. Patil**[1,4,5,6], **Dawen Cai**[6,7,8], **Cynthia A. Chestek**[1,6,9,10,‡]

[1]Department of Biomedical Engineering, University of Michigan, Ann Arbor, MI 48109, United States of America

[2]Department of Molecular, Cellular, and Developmental Biology, University of Michigan, Ann Arbor, MI 48019, United States of America

[3]Department of Mechanical Engineering, University of Michigan, Ann Arbor, MI 48109, United States of America

[4]Department of Neurosurgery, University of Michigan Medical School, Ann Arbor, MI 48109, United States of America

[5]Department of Neurology, University of Michigan Medical School, Ann Arbor, MI 48109, United States of America

[6]Neuroscience Graduate Program, University of Michigan Medical School, Ann Arbor, MI 48109, United States of America

[7]Department of Biophysics, University of Michigan, Ann Arbor, MI 48109, United States of America

[8]Department of Cell and Developmental Biology, University of Michigan Medical School, Ann Arbor, MI 48019, United States of America

[9]Department of Electrical Engineering and Computer Science, University of Michigan, Ann Arbor, MI 48109, United States of America

[10]Robotics Program, University of Michigan, Ann Arbor, MI 48109, United States of America

Abstract

Objective.—The Utah array is widely used in both clinical studies and neuroscience. It has a strong track record of safety. However, it is also known that implanted electrodes promote the formation of scar tissue in the immediate vicinity of the electrodes, which may negatively impact

‡ Corresponding author: cchestek@umich.edu.

* Co-first authors

Author Contributions

PRP, EJW, HS, AJB, DC, and CAC designed the study. EJW, HS, PRP, and JGL analyzed the histological data. PRP, AVM, and CMC processed, stained, and imaged the tissue. EJW, JMR, and HET, analyzed and scored explanted arrays. PGP performed the NHP surgeries. All authors approved the final manuscript.

the ability to record neural waveforms. This scarring response has been primarily studied in rodents, which may have a very different response than primate brain.

Approach.—Here, we present a rare nonhuman primate histological dataset (n=1 rhesus macaque) obtained 848 and 590 days after implantation in two brain hemispheres. For 2 of 4 arrays that remained within the cortex, NeuN was used to stain for neuron somata at 3 different depths along the shanks. Images were filtered and denoised, with neurons then counted in the vicinity of the arrays as well as a nearby section of control tissue. Additionally, 3 of 4 arrays were imaged with a scanning electrode microscope (SEM) to evaluate any materials damage that might be present.

Main results.—Overall, we found a 63% percent reduction in the number of neurons surrounding the electrode shanks compared to control areas. In terms of materials, the arrays remained largely intact with metal and Parylene C present, though tip breakage and cracks were observed on many electrodes.

Significance.—Overall, these results suggest that the tissue response in the nonhuman primate brain shows similar neuron loss to previous studies using rodents. Electrode improvements, for example using smaller or softer probes, may therefore substantially improve the tissue response and potentially improve the neuronal recording yield in primate cortex.

1. Introduction

Brain-machine interfaces (BMIs) offer patients living with motor or sensory impairments – often resulting from injuries to the spinal cord, nerves or muscles – the chance to regain movement or restore sensation [1–3]. State-of-the-art BMIs require invasive technology that rests on direct electrical connection between healthy neural tissue and an external computer. Users of BMIs have independently fed themselves a drink [4], felt the touch of a loved one [5,6], controlled the movement of their own physically reanimated arm [7], regained touch-pressure sensation [8], and fist-bumped a former U.S. president [9]. This rapidly expanding list of BMI capabilities is enabled by engineering breakthroughs, such as sophisticated decoding algorithms that extract useful information from noisy data, or low-power amplifiers that facilitate analysis of brain signals with a fraction of the computational bandwidth previously needed [10,11]. What has remained constant is the neural device responsible for interfacing directly with the brain's cortex, the Utah Electrode Array (UEA) [12], which is the only intracortical device approved for clinical BMIs [13].

Despite the longest running clinical BMI study lasting approximately 5.4 years, the majority of BMI studies report a worsening of two key measurements within months to one year after UEA implant: a decrease in recorded amplitude of electrical signals from individual or small groups of neurons, and a decrease in the total number of working electrodes on the UEA [14] [15–17]. Poor quality neural signals and low numbers of working electrodes limit the progress of BMIs towards the goal of replicating natural, high-precision movements and sensory inputs for BMI users [18].

There may be several reasons for the limited quality and quantity of neural signals recorded on UEAs. Studies of long-term UEA implants in brain tissue report fewer neurons and more tissue scarring and inflammation near electrode shanks [19–25]. In 2005, Biran,

Martin, and Tresco published observations of the density of neurons around silicon shank electrodes, which are similar to Utah array shanks in size and material, and determined a decrease in neural density extending roughly 200 μm from the surface of a silicon shank [26]. In UEAs, this distance would affect the entire recording region between two adjacent electrodes that sit 400 μm apart [27]. In addition to possible decreases in neuronal density, the UEA electrodes appear to degrade under the constant exposure to the warm, watery, and high-salinity environment in the brain [28]. Reactive oxygen species0020– which are linked to the degradation of electrical devices – were found in elevated numbers inside the scar region that was shown to form around silicon electrodes [29]. Extensive scar tissue and resulting encapsulation of UEAs in peripheral nerves were found to lead to Parylene C delamination, cracking, and thinning, as well as cracking of the conductive electrode coating [28,30].

Much of the data on UEA degradation and the foreign body response was gathered in feline or rodent models [20,25,31–33], leaving the obvious question of what occurs during human clinical trials. A recent study on explanted UEAs after 0.5 and 2.7 years in the cortex of two BMI patients looked at the signal quality and material degradation, and found greater tissue encapsulation and worsening electrode coating degradation exhibited on longer implants [34]. Similarly, histopathology of tissue surrounding two UEAs in one patient confirmed similar scarring and widespread necrosis seen previously in animal models that correlated with signal degradation [35]. However, clinical trials are rare as is the histological analysis of human brain tissue. Non-human primates (NHPs) are often used to test advanced BMIs as a substitute to human patients.

One group, led by John Donoghue, examined the biological, material, and mechanical failure modes of UEAs after long-term implantation in the cortex of over two dozen NHPs [15]. In this study, approximately 80% of UEAs failed completely while implanted, the majority of which failed within the first year of implant [15]. Although thorough, this study was limited to whole-electrode failures, such as meningeal encapsulation or wire breakage [15]. To expand on this work, the group then examined explanted UEAs with gross histology and SEM imaging [36]. The tissue and electrode images showed a substantial presence of inflammatory markers, a minimal change in neuron density near the electrode holes, and overall signs of material fatigue and degradation of the arrays [36]. These two studies laid the groundwork for understanding why and how UEAs fail in long-term brain implantation. However, the histology was limited due to the qualitative analysis and because the arrays were either completely or mostly pushed out of the brain and therefore not representative of arrays that remain implanted over chronic time periods [36]. Furthermore, observations from the SEM were also qualitative [36]. Therefore, a study quantifying changes in neuron density near shank holes coupled with a quantitative visual analysis of the electrodes' material degradation is still needed.

Here, we add to the collective knowledge of changes in neuronal density and UEA integrity after multi-year implantation in a rare dataset from the cortex of one NHP. We analyze the neuron density surrounding UEA explant sites in the sensory cortices in both the left and right hemispheres after 2.3 and 1.6 years, respectively. The neuron density around electrode shank holes is compared to nearby non-implanted tissue to quantify the change

induced by UEA presence. We expand upon previous preliminary analysis of neuron density counted manually by introducing a semi-automated counting methodology applied to all electrode shank holes [37]. We also analyze images of the UEAs using scanning electron microscopy (SEM) to determine changes in the electrode surface and the spatial arrangement of degradation within the array. This study furthers our understanding of long-term UEA implantation in the cortex of an NHP, moving the field one step closer to understanding the implication of clinical BMI use.

2. Methods

2.1 Experimental set-up

This study examines the histological tissue response and material changes of four UEAs (Blackrock Microsystems, Salt Lake City, UT) implanted in the sensory and motor cortices of a single rhesus macaque NHP (Figure 1). The NHP was involved in a BMI study and trained for brain control tasks of individual finger movements [38,39]. The NHP was also involved in corticocortical processing experiments using ketamine [40]. The NHP was euthanized at the termination of these experimental timelines due to successful completion of experimental objectives coupled with deteriorating health. The UEAs were extracted, cleaned, imaged, and analyzed for material changes. The brain tissue under the UEAs was sliced, stained, imaged, and analyzed for changes in neuron density.

2.2 UEA implantation

All animal procedures were approved by the University of Michigan Institutional Animal Care & Use Committee. Two UEAs were implanted in the primary motor (M1) and sensory (S1) cortex of each hemisphere. The left hemisphere was implanted on August 20, 2015 (Figure 1A–C) and the right hemisphere on May 4, 2016 (Figure 1D, E). Each UEA was of standard architecture: 100 electrodes at the tips of 1.5 mm-long shanks and a 6 cm length wire bundle. The electrode tips of three UEAs were coated with iridium oxide and implanted in the left motor (LM), left sensory (LS), and right sensory (RS) cortices. The right motor cortex (RM) was implanted with a UEA with platinum-coated electrode tips. The UEAs in left and right sensory cortices were fabricated with an experimental aluminum oxide coating prior to Parylene C insulation [41].

The NHP was placed in a stereotaxic frame after induction with general anesthesia during each implantation surgery. The location of the craniotomy over the central sulcus was estimated using the stereotaxic setup and a craniotomy and durotomy were performed over the region of implant. The UEAs were manually positioned and then impacted into the cortical tissue using a pneumatic inserter (Blackrock Microsystems, Salt Lake City, UT), seen in Figure 1A and 1D. The dura was closed over the UEAs and sealed with PRECLUDE Pericardial Membrane (Gore, Flagstaff, AZ) and DuraGen (Integra LifeSciences, Princeton, NJ). The bone flap was replaced and fastened with titanium bone screws (DePuy Synthes, Paoli, PA). Silicone elastomer (KwikCast, World Precision Instruments, Sarasota, FL) and dental acrylic (A-M Systems, Sequim, WA) were applied to secure the wire bundles to the skull.

2.3 UEA and brain tissue extraction

All four UEAs were extracted on December 15, 2017, after 848 days of implantation in the left hemisphere (Figure 1B, C) and 590 days of implantation in the right hemisphere (Figure 1E). The terminal surgical extraction protocol required that perfusion not be performed while the NHP was under anesthesia. Therefore, post-mortem perfusion began approximately 4 minutes after death, as confirmed by veterinary staff. The NHP was anesthetized with ketamine and then sacrificed with euthanasia solution (VetOne, Boise, ID). The NHP was then transcardially perfused with heparinized (10 U/mL) 1X phosphate buffered saline (PBS) solution (BP3994, Fisher, Waltham, MA) until the exudate was clear, followed by approximately 1 L of 4% (w/v) paraformaldehyde (PFA) fixative (19208, Electron Microscopy Sciences, Hatfield, PA) in 1X PBS.

After perfusion, the dental acrylic and overlying bone flap were removed with a handheld drill. Dural growth on top of the UEAs was removed. The brain sections containing the UEAs were excised and placed in 4% PFA for 72 hours at 4 °C (Figure 1B, E). At this point the UEAs were removed with fine forceps and immediately placed in a chemical disinfectant (Benz-All, Xttrium Laboratories, Inc., Mount Prospect, IL) overnight. UEAs were switched to 1X PBS after approximately 24 hours to be preserved for future analysis. After UEA extraction, the brain sections were returned to 4% PFA for an additional 48 hours at 4 °C and then stored in 1X PBS at 4 °C.

2.4 Tissue slicing

Brain sections were trimmed of excess tissue and the implant portions were separated from each other. The implant portions were placed in 4% PFA for 5 days followed by 8 days in 1X PBS at 4 °C. Implant portions were cryoprotected in 30% sucrose (S0389, Sigma Aldrich, St. Louis, MO) in 1X PBS at 4 °C for 26 days and then frozen at −80 °C in optimal cutting temperature compound (Tissue-Tek, Sakura Finetek USA, Inc., Torrance, CA). The tissue was sliced perpendicular to the implantation sites in 100 μm thick sections at −16 °C on a cryostat. Tissue slices were stored in 0.02% sodium azide (DSS24080, Dot Scientific Inc., Burton, MI) in 1X PBS at 4 °C until immunohistochemical labeling. Throughout this study slices are referred to by their final depth in hundreds of microns from the surface of the brain. For example, slice 13 contains tissue 1200–1300 μm from the top of the implant portion.

2.5 Tissue staining

Slices at varying depths down the UEA shank were selected for tissue staining. Tissue slices were blocked and permeabilized with a mixture of StartingBlock PBS Blocking Buffer (37538, Thermo Scientific, Waltham, MA) and 1% Triton X-100 (9002-93-1, Sigma Aldrich, St. Louis, MO) overnight at 4 °C followed by three 30-minute washes in 1X PBS containing 0.5% Triton X-100, referred to as 0.5% PBST, at room temperature. The tissue was incubated with primary antibody at a 1:250 dilution in 0.5% PBST with 0.02% sodium azide for 48 hours at 4 °C. The following primary antibody was used to stain for neurons, mouse anti-neuronal nuclei (NeuN, MAB377, MilliporeSigma, Burlington, MA). Primary antibody incubation was followed by three 30-minute washes in 0.5% PBST at room temperature. The tissue was incubated in secondary antibody at a 1:250 dilution

in 0.5% PBST with 0.02% sodium azide for 24 hours at 4 °C. The following secondary antibody was used, anti-mouse Alexa Fluor 647 (715-605-150, Jackson ImmunoResearch Laboratories, Inc., Carlsbad, CA). Finally, the tissue slices were washed in room temperature 0.5% PBST two times at two-hour intervals and kept in 1X PBS overnight. All slices were stored at 4 °C in 1X PBS with 0.02% sodium azide until imaged.

2.6 Tissue imaging

Tissue slices were imaged on a Zeiss LSM 780 Confocal Microscope (Carl Zeiss AG, Oberkochen, Germany) with a 20X objective. Images were collected with an approximately 0.4–0.6 μm X and Y pixel size and 2 μm z-step for the total 100 μm depth of the slice. The NeuN stain was imaged at a wavelength of 633 nm (NeuN). Laser intensity was adjusted manually to prevent pixel saturation, corrected in the Z direction to also prevent saturation, and ranged from 1.2–80% laser power. The gain and contrast were altered during image processing in ImageJ.

2.7 Tissue analysis

Neuron density around electrode shank site was calculated from the NeuN tissue images and compared to the neuron density in non-implanted tissue. Viable non-implant tissue sites were selected in areas outside regions of visible damage. Electrode shank site and non-implant tissue regions were cropped to 400 μm by 400 μm sections in MATLAB (Mathworks, Natick, MA) centering on the electrode shank hole. The image depth was cropped to the center 40 or 70 μm of the 100 μm-thick slice. The total 3D volume was 6.4×10^6 μm^3 or 11.2×10^6 μm^3. For each electrode shank site image, a circle was manually fit to the electrode shank hole across its z-stack in ImageJ (U.S. National Institutes of Health, Bethesda, MD). The volume of a cylinder with the same radius was subtracted from the total 3D volume to account for the electrode shank's volume.

Each cropped image was pre-processed in ImageJ. The pixel intensity was normalized across z-stacks to the highest signal-to-noise ratio z-step using the histogram matching feature [42]. The image was filtered with a mean 50-pixel filter and the background was subtracted to remove pixelated noise. The image was then denoised with a 3D Gaussian 2-pixel radius filter to remove individual pixels with abnormally high intensity.

Then, the pre-processed image was read into MATLAB for 3D visualization using the Volume Viewer application. A 3D view of the neurons was generated using the isosurface feature with a unique isosurface value for each slice, as determined by a trained operator to accurately match the original image. A 2D image of the slice was imported back into ImageJ for cell counting. The image was smoothed and converted to 8-bit grayscale. The range of particle sizes used to identify neurons was determined by a trained operator measuring the smallest and largest neurons. The Analyze Particles program was run to locate neurons and a trained operator reviewed the resulting identifications for misidentified or unidentified neurons. The neuron density was calculated by dividing the total neuron count by the remaining image volume.

2.8 UEA scanning electron microscopy imaging

To determine if there was any electrode degradation, UEAs were cleaned and imaged. First, UEAs were removed from 1X PBS and soaked in deionized water for 1 hour to detach any remaining brain tissue. UEAs were air dried for 1 hour prior to affixation to SEM stubs (16111, Ted Pella, Redding, CA) with carbon tape (16073, Ted Pella, Redding, CA). UEAs were imaged in a TESCAN Rise SEM (Tescan Orsay Holding, Brno–Kohoutovice, Czech Republic) at 20 kV using the low vacuum secondary detector. UEAs were tilted to approximately 20 degrees for maximum visibility of electrode tips. Images were collected of the whole array and of each quadrant of 5×5 electrode shanks. Backscatter mode images were also collected to detect cracks in the Parylene C insulation.

2.9 Electrode analysis

Images of each UEA quadrant of 5×5 electrode shanks were analyzed for six categories of degradation: electrode tip breakage (TB), cracks in metal electrode coating (CC), below-electrode tip shank fracture (SF), unidentified or abnormal debris (AB), Parylene C cracks (PC) and Parylene C peeling or delamination (PD). Examples of each category are shown in Figure 3B as identified on LS (Figure 3A), except for Parylene C delamination which was found on RM. Three trained operators scored each shank as exhibiting (1) or not exhibiting (0) the degradation category. Scores were averaged across operators and then rounded to 0 or 1. The outer three rows of electrode shanks were statistically compared to the inner 4×4 electrode shanks in an ANOVA test (alpha < 0.05). Analysis was conducted using MATLAB.

3. Results

3.1 Analysis of neuron density

We analyzed the tissue slices found under the LS array at three depths along the length of electrode shanks at 800–900 μm, 1000–1100 μm, and 1200–1300 μm and under the RS array at 1600–1700 μm, 1700–1800 μm, and 2000–2100 μm. Figure 2 depicts the electrode shank (Figure 2B) and non-implanted tissue (Figure 2C) regions of interest analyzed in slice 11 for the LS array (Figure 2A). Representative images of the three main stages of the analysis are shown in Figure 2B and 2C: the original image (top), the image after filtering and processing (middle), and the image analyzed with Analyze Particles in ImageJ (bottom).

For the LS array we determined a non-implanted tissue density of 40.4×10^3 neurons/mm^3 for the slice at an estimated 800–900 μm depth, 33.8×10^3 neurons/mm^3 for the slice at an estimated 1000–1100 μm depth, and 38.2×103 neurons/mm3 for the slice at an estimated 1200–1300 μm depth. In comparison, there were fewer neurons in the tissue around the electrode shank holes. We calculated a mean neuron density of 13.9×103 ± 9.6×103 neurons/mm3 surrounding the 393 intact electrode shank holes from the six slices. We measured neuron density reductions of 74%, 57%, and 78% around the electrode shank holes compared to the non-implant tissue at 800–900 μm, 1000–1100 μm, 1200–1300 μm depths for the LS array. The neuron density surrounding the electrode shank holes was reduced by an average of 63% compared to the nearby non-implanted tissue. Additionally, we sought to determine whether tissue near shank tips had improved neuron densities. We

measured the neuron density at a depth of approximately 1700–1800 μm of six holes that rapidly disappeared in subsequent slices, indicating their proximity to the tips. We found a neuron density of $16.2\times10^3\pm 9.2\times10^3$ neurons/mm^3, which was close to the density measured across all electrode shanks.

3.2 Analysis of UEA electrode shanks

SEM images were collected of the four Utah arrays to identify visible damage or degradation to the electrode shanks. One experimental array (LM) was excluded from the characterization study due to a complete lack of Parylene C and tip coating. We quantified the occurrence of the six degradation categories over the three arrays (N=300 electrode shanks), shown in Figure 3C. When ranked from most to least present, the six categories were Parylene C cracks (40.3%), coating cracks (39.7%), tip breakage (22.3%), shank fracture (3.3%), abnormal debris (1.7%), and Parylene C delamination (1.3%). Of all examined electrode shanks, 112 electrode shanks or 37.3% exhibited visible to no degradation.

We analyzed the spatial arrangement of each degradation by performing a 1-way ANOVA test comparing the occurrence of degraded shanks in the outermost three rows of electrode shanks to the innermost 4×4 square of electrode shanks (Figure 3A, dashed white box). There was a significant difference between the outer and inner electrode shanks for the coating cracks ($p=0.003$) and tip breakage ($p=0.004$).

4. Discussion

In the present study, we explored UEA longevity in the brain through histological analysis of NHP cortex and examination of the mechanical degradation of UEAs implanted for 1.6 and 2.3 years in the brain. The purpose of this study was to enrich our understanding of failure mechanisms in long-term BMIs, which rely on brain signals recorded by UEAs.

Here, we calculated the neuron density surrounding the electrode shank holes and nearby non-implanted tissue. We found a 63% decrease in neuron density surrounding UEA shanks (13.9×10^3 neurons/mm^3) compared to that of nearby non-implanted tissue (37.4×10^3 neurons/mm^3). The considerable reduction in neuron density that we observed is evidence in NHPs of a drastic disruption in neural populations, which has previously been observed in rodents implanted with rodent UEAs [24,25] and with multi-shank Michigan electrodes [43]. Many previous studies have examined the formation of a scar around chronically implanted UEAs [44] but few have quantified the effect UEAs have on the nearby neuron population in NHPs [15,36,45–47]. The neuron density of non-implanted tissue found here is on the same order of magnitude as those in previous studies that found a non-implanted neuron density in the primary motor (66×10^3 neurons/mm^3) and primary somatosensory (101×10^3 neurons/mm^3) areas of the marmoset NHP cortex [48]. Our preliminary observations note a dramatic decrease in neurons within the immediate recording radius of the electrode shanks, indicating signal loss from long-term UEA usage may be due to a lack of neurons. However, given that the tissue measured in this study did not capture the electrode tips, it may be possible that neuron density reductions were less in more ventral depths where the shank was thinner and perhaps caused less damage, although our preliminary analyses of a small

subset of near-tip holes and inspection of the tissue below these holes suggest that this is not necessarily the case.

This study also evaluated SEM images of the extracted UEAs for tip breakage, tip coating cracking, shank fracture, abnormal debris, Parylene C delamination, and Parylene C cracking. Tip breakage, coating cracking, and Parylene C cracking appeared on 20–40% of the electrode shanks, while shank fracture, abnormal debris, and Parylene C delamination appeared on fewer than 4% of shanks. A concentration of degradation at the most vulnerable portion of the electrode shank, the electrode tip, is expected. However, Parylene C cracking would indicate a substantial decrease in electrical impedance, which we did not see from both anecdotal evidence and inspection of impedance changes over time. The Parylene C cracks may be a result of the pressure within the SEM, despite being imaged under low vacuum, but this would indicate the silicon shank had detached from the Parylene C coating, another cause for electrical impedance change.

We found a significant difference in the number of electrode shanks exhibiting tip breakage and coating cracks on the outer perimeter of the UEA as compared to the inner region. This may be explained by lateral stresses placed on the outermost electrode shanks when pulled by the wire bundle or micromotion of the brain. Shank fracture, while occurring on just 3% of electrode shanks, may be partially or entirely explained by post-mortem extraction. Our surgical notes indicate that some shank fracture may have occurred during extraction from the fixed tissue, although a precise number is not known. Additionally, the manufacturer (Blackrock Microsystems) certified that each array had a maximum of five broken channels, although the exact number, if any, was not specified. We do not believe that any shanks were damaged during insertion, based on recent work that observed no breakage when performing insertion testing with Utah Slanted Electrode Arrays, which have comparable geometry and require similar pneumatic insertion [49].

We attempted to identify how these different damage categories might have affected recording capabilities by analyzing impedances that were measured over time. However, these impedances showed no clear trend or noticeable differences compared to the array as a whole over time or in the final measurements. This was also the case when we compared impedances of electrodes situated in the inner region against those along the outer perimeter. Furthermore, impedances for the RM and LS arrays were last measured months before euthanasia and these values may not reflect the arrays' final state of degradation.

While this study furthers our knowledge on the impact of chronic UEA implantation, it is also limited. The most obvious limitation is the single NHP used in this study. Higher-order animal models are invaluable to clinical research and studies are constructed to maximize the lifespan and usefulness of each animal. This minimizes access to NHP brain tissue surrounding chronically implanted UEAs [15,36]. This study was also limited in the number of UEAs implanted in the single NHP. Four UEAs were implanted, one per cortical region of interest in each hemisphere. However, upon termination, one array was discovered to be fully encapsulated in fibrotic tissue. Previous studies have examined the fibrotic tissue response to implanted silicon electrodes and found that fibrotic encapsulation is not an unusual outcome for long term implants in brain [15,36,50] or nerve tissue [51]. However,

few studies have examined the encapsulated UEA for damage or degradation [28]. This study found that the encapsulated UEA was devoid of metal tip coating material or Parylene C insulation, despite the silicon structure remaining otherwise intact. It is possible that the reactive oxygen species in the fibrotic encapsulation caused severe degradation of the Parylene C and metal tip coating, while the fibrotic tissue provided a buffer against physical damage [29].

This study is also limited by the available stained tissue, which constrained the location of non-implant tissue to an area just outside the UEA footprint. While our neuron density of non-implanted tissue aligns with previous records of healthy NHP cortex neuron density [48], the region may still be impacted by the nearby UEA in ways unknown to us [52]. Additionally, the depth of the tissue slices along the length of the electrode shank is not precisely known. We identified the tissue depth as relative to the surface of the brain for that specific tissue section. However, the tissue surface can be irregular or cratered, making it difficult to know the exact depth of the tissue slice. Additionally, we were mostly unable to identify the end of the shank hole within the stained tissue slices. We choose to analyze slices that depicted obvious shank holes, but this limits our ability to know the distance between the recording region and the neurons in the slices analyzed here.

5. Conclusion

This study elucidates the effects of UEAs chronically implanted in the motor and sensory cortices of an NHP. While mechanical degradation occurred on 20–40% of electrode shanks, neuronal loss of nearly 63% near the electrode shanks likely contributes more to signal attenuation. This suggests that BMI performance may be more limited by a lack of nearby neurons than material failures of UEAs. Fortunately, a major goal of newer electrode designs is increased biocompatibility [22,53,54] to improve neuronal health. Designs with smaller sizes and reduced stiffness have shown immense promise [22,53,55–59]. This work provides further evidence that newer, more biocompatible electrodes must next be tested in conjunction with BMIs for the electrodes to become a suitable clinical option.

Acknowledgments

This work was financially supported by the National Institute of General Medical Sciences (R01GM111293), the National Institute of Neurological Disorders and Stroke (UF1NS107659), and the National Science Foundation (1707316). The authors would like to thank Matthew Mender and Joseph Costello for their assistance with the impedance data analysis.

References

[1]. Collinger JL, Wodlinger B, Downey JE, Wang W, Tyler-Kabara EC, Weber DJ, McMorland AJ, Velliste M, Boninger ML and Schwartz AB 2013 High-performance neuroprosthetic control by an individual with tetraplegia Lancet 381 557–64 [PubMed: 23253623]

[2]. Davis TS, Wark HAC, Hutchinson DT, Warren DJ, O'Neill K, Scheinblum T, Clark GA, Normann RA and Greger B 2016 Restoring motor control and sensory feedback in people with upper extremity amputations using arrays of 96 microelectrodes implanted in the median and ulnar nerves J. Neural Eng. 13

[3]. Page DM, George JA, Kluger DT, Duncan C, Wendelken S, Davis T, Hutchinson DT and Clark GA 2018 Motor Control and Sensory Feedback Enhance Prosthesis Embodiment and Reduce Phantom Pain After Long-Term Hand Amputation Front. Hum. Neurosci. 12

[4]. Hochberg LR, Bacher D, Jarosiewicz B, Masse NY, Simeral JD, Vogel J, Haddadin S, Liu J, Cash SS, van der Smagt P and Donoghue JP 2012 Reach and grasp by people with tetraplegia using a neurally controlled robotic arm Nature 485 372–5 [PubMed: 22596161]

[5]. Wang W, Degenhart AD, Holder DL, Louis S and Moran DW 2011 Human Motor Cortical Activity Recorded with Micro-ECoG Electrodes During Individual Finger Movements 1–9

[6]. Srikameswaran A 2011 Man With Spinal Cord Injury Uses Brain-Computer Interface to Move Prosthetic Arm With His Thoughts PittChronicle

[7]. Ajiboye AB, Willett FR, Young DR, Memberg WD, Murphy BA, Miller JP, Walter BL, Sweet JA, Hoyen HA, Keith MW, Peckham PH, Simeral JD, Donoghue JP, Hochberg LR and Kirsch RF 2017 Restoration of reaching and grasping movements through brain-controlled muscle stimulation in a person with tetraplegia: a proof-of-concept demonstration Lancet 389 1821–30 [PubMed: 28363483]

[8]. Flesher SN, Collinger JL, Foldes ST, Weiss JM, Downey JE, Tyler-Kabara EC, Bensmaia SJ, Schwartz AB, Boninger ML and Gaunt RA 2016 Intracortical microstimulation of human somatosensory cortex Sci. Transl. Med. 8 1–10

[9]. Souza P 2016 President Obama fist-bumps Nathan Copeland Obama White House

[10]. Ludwig KA, Miriani RM, Langhals NB, Joseph MD, Anderson DJ and Kipke DR 2009 Using a common average reference to improve cortical neuron recordings from microelectrode arrays J. Neurophysiol. 101 1679–89 [PubMed: 19109453]

[11]. Nason SR, Vaskov AK, Willsey MS, Welle EJ, An H, Vu PP, Bullard AJ, Nu CS, Kao JC, Shenoy KV., Jang T, Kim HS, Blaauw D, Patil PG and Chestek CA 2020 A low-power band of neuronal spiking activity dominated by local single units improves the performance of brain–machine interfaces Nat. Biomed. Eng. 4 973–83 [PubMed: 32719512]

[12]. Nordhausen CT, Maynard EM and Normann RA 1996 Single unit recording capabilities of a 100 microelectrode array Brain Res. 726 129–40 [PubMed: 8836553]

[13]. Normann RA and Fernandez E 2016 Clinical applications of penetrating neural interfaces and Utah Electrode Array technologies J. Neural Eng. 13

[14]. Masse NY, Jarosiewicz B, Simeral JD, Bacher D, Stavisky SD, Cash SS, Oakley EM, Berhanu E, Eskandar E, Friehs G, Hochberg LR and Donoghue JP 2014 Non-causal spike filtering improves decoding of movement intention for intracortical BCIs J. Neurosci. Methods 236 58–67 [PubMed: 25128256]

[15]. Barrese JC, Rao N, Paroo K, Triebwasser C, Vargas-Irwin C, Franquemont L and Donoghue JP 2013 Failure mode analysis of silicon-based intracortical microelectrode arrays in non-human primates J. Neural Eng. 10 066014 [PubMed: 24216311]

[16]. Simeral JD, Kim SP, Black MJ, Donoghue JP and Hochberg LR 2011 Neural control of cursor trajectory and click by a human with tetraplegia 1000 days after implant of an intracortical microelectrode array J. Neural Eng. 8

[17]. Bullard AJ, Hutchison BC, Lee J, Chestek CA and Patil PG 2020 Estimating Risk for Future Intracranial, Fully Implanted, Modular Neuroprosthetic Systems: A Systematic Review of Hardware Complications in Clinical Deep Brain Stimulation and Experimental Human Intracortical Arrays Neuromodulation 23 411–26 [PubMed: 31747103]

[18]. Sponheim C, Papadourakis V, Collinger JL, Downey J, Weiss J, Pentousi L, Elliott K and Hatsopoulos NG 2021 Longevity and reliability of chronic unit recordings using the Utah, intracortical multi-electrode arrays J. Neural Eng. 18

[19]. Biran R, Martin DC and Tresco PA 2007 The brain tissue response to implanted silicon microelectrode arrays is increased when the device is tethered to the skull J. Biomed. Mater. Res. - Part A 82 169–78

[20]. Karumbaiah L, Saxena T, Carlson D, Patil K, Patkar R, Gaupp EA, Betancur M, Stanley GB, Carin L and Bellamkonda RV. 2013 Relationship between intracortical electrode design and chronic recording function Biomaterials 34 8061–74 [PubMed: 23891081]

[21]. Kozai TDY, Catt K, Li X, Gugel ZV., Olafsson VT, Vazquez AL and Cui XT 2015 Mechanical failure modes of chronically implanted planar silicon-based neural probes for laminar recording Biomaterials 37 25–39 [PubMed: 25453935]

[22]. Salatino JW, Ludwig KA, Kozai TDY and Purcell EK 2017 Glial responses to implanted electrodes in the brain Nat. Biomed. Eng. 1 862–77 [PubMed: 30505625]

[23]. Potter KA, Buck AC, Self WK and Capadona JR 2012 Stab injury and device implantation within the brain results in inversely multiphasic neuroinflammatory and neurodegenerative responses J. Neural Eng. 9

[24]. Nolta NF, Christensen MB, Crane PD, Skousen JL and Tresco PA 2015 BBB leakage, astrogliosis, and tissue loss correlate with silicon microelectrode array recording performance Biomaterials 53 753–62 [PubMed: 25890770]

[25]. Black BJ, Kanneganti A, Joshi-Imre A, Rihani R, Chakraborty B, Abbott J, Pancrazio JJ and Cogan SF 2018 Chronic recording and electrochemical performance of utah microelectrode arrays implanted in rat motor cortex J. Neurophysiol. 120 2083–90 [PubMed: 30020844]

[26]. Biran R, Martin DC and Tresco PA 2005 Neuronal cell loss accompanies the brain tissue response to chronically implanted silicon microelectrode arrays Exp. Neurol. 195 115–26 [PubMed: 16045910]

[27]. Henze DA, Borhegyi Z, Csicsvari J, Mamiya A, Harris KD and Buzsáki G 2000 Intracellular features predicted by extracellular recordings in the hippocampus in vivo J. Neurophysiol. 84 390–400 [PubMed: 10899213]

[28]. Caldwell R, Street MG, Sharma R, Takmakov P, Baker B and Rieth L 2020 Characterization of Parylene-C degradation mechanisms: In vitro reactive accelerated aging model compared to multiyear in vivo implantation Biomaterials 232 119731 [PubMed: 31918225]

[29]. Ereifej ES, Rial GM, Hermann JK, Smith CS, Meade SM, Rayyan JM, Chen K, Feng H and Capadona JR 2018 Implantation of neural probes in the brain elicits oxidative stress Front. Bioeng. Biotechnol. 6

[30]. Shafer B, Welle C and Vasudevan S 2019 A rat model for assessing the long-term safety and performance of peripheral nerve electrode arrays J. Neurosci. Methods 328 108437 [PubMed: 31526764]

[31]. Szarowski DH, Andersen MD, Retterer S, Spence AJ, Isaacson M, Craighead HG, Turner JN and Shain W 2003 Brain responses to micro-machined silicon devices Brain Res. 983 23–35 [PubMed: 12914963]

[32]. Ward MP, Rajdev P, Ellison C and Irazoqui PP 2009 Toward a comparison of microelectrodes for acute and chronic recordings Brain Res. 1282 183–200 [PubMed: 19486899]

[33]. McCreery D, Cogan S, Kane S and Pikov V 2016 Correlations between histology and neuronal activity recorded by microelectrodes implanted chronically in the cerebral cortex J. Neural Eng. 13 36012

[34]. Woeppel K, Hughes C, Herrera AJ, Eles JR, Tyler-Kabara EC, Gaunt RA, Collinger JL and Cui XT 2021 Explant Analysis of Utah Electrode Arrays Implanted in Human Cortex for Brain-Computer-Interfaces Front. Bioeng. Biotechnol. 9 1–15

[35]. Szymanski LJ, Kellis S, Liu CY, Jones KT, Andersen RA, Commins D, Lee B, McCreery DB and Miller CA 2021 Neuropathological effects of chronically implanted, intracortical microelectrodes in a tetraplegic patient J. Neural Eng. 18 0460b9

[36]. Barrese JC, Aceros J and Donoghue JP 2016 Scanning electron microscopy of chronically implanted intracortical microelectrode arrays in non-human primates J. Neural Eng. 13

[37]. Bullard AJ 2019 Feasibility of Using the Utah Array for Long-Term Fully Implantable Neuroprosthesis Systems (University of Michigan)

[38]. Irwin ZT, Schroeder KE, Vu PP, Bullard AJ, Tat DM, Nu CS, Vaskov A, Nason SR, Thompson DE, Bentley JN, Patil PG and Chestek CA 2017 Neural control of finger movement via intracortical brain-machine interface J. Neural Eng. 14

[39]. Vaskov AK, Irwin ZT, Nason SR, Vu PP, Nu CS, Bullard AJ, Hill M, North N, Patil PG and Chestek CA 2018 Cortical decoding of individual finger group motions using ReFIT Kalman filter Front. Neurosci. 12

[40]. Schroeder KE, Irwin ZT, Gaidica M, Bentley JN, Patil PG, Mashour GA and Chestek CA 2016 Disruption of corticocortical information transfer during ketamine anesthesia in the primate brain Neuroimage 134 459–65 [PubMed: 27095309]

[41]. Xie X, Rieth L, Cardwell R, Sharma R, Yoo JM, Diweka M, Tathireddy P and Solzbacher F 2013 Bi-layer encapsulation of utah array based nerual interfaces by atomic layer deposited Al2O3 and parylene C 2013 Transducers Eurosensors XXVII 17th Int. Conf. Solid-State Sensors, Actuators Microsystems, TRANSDUCERS EUROSENSORS 2013 1267–70

[42]. Miura K 2020 Bleach correction ImageJ plugin for compensating the photobleaching of time-lapse sequences F1000Research 9 1–17

[43]. Welle CG, Gao YR, Ye M, Lozzi A, Boretsky A, Abliz E and Hammer DX 2020 Longitudinal neural and vascular structural dynamics produced by chronic microelectrode implantation Biomaterials 238 119831 [PubMed: 32045783]

[44]. Christensen MB, Pearce SM, Ledbetter NM, Warren DJ, Clark GA and Tresco PA 2014 The foreign body response to the Utah Slant Electrode Array in the cat sciatic nerve Acta Biomater. 10

[45]. Malaga KA, Schroeder KE, Patel PR, Irwin ZT, Thompson DE, Nicole Bentley J, Lempka SF, Chestek CA and Patil PG 2016 Data-driven model comparing the effects of glial scarring and interface interactions on chronic neural recordings in non-human primates J. Neural Eng. 13

[46]. House PA, MacDonald JD, Tresco PA and Normann RA 2006 Acute microelectrode array implantation into human neocortex: preliminary technique and histological considerations. Neurosurg. Focus 20 19–22

[47]. Rousche PJ and Normann RA 1998 Chronic recording capability of the utah intracortical electrode array in cat sensory cortex J. Neurosci. Methods 82 1–15 [PubMed: 10223510]

[48]. Atapour N, Majka P, Wolkowicz IH, Malamanova D, Worthy KH and Rosa MGP 2019 Neuronal Distribution across the Cerebral Cortex of the Marmoset Monkey (Callithrix jacchus) Cereb. Cortex 29 3836–63 [PubMed: 30357325]

[49]. Thomas WM, Leber M, Crew J and Warren DJ 2022 Evaluation of Pneumatic Insertion Stability of Utah Slanted Electrode Arrays in Rat Sciatic Nerve Annu. Int. Conf. IEEE Eng. Med. Biol. Soc. IEEE Eng. Med. Biol. Soc. Annu. Int. Conf. 2022 5099–102

[50]. Cody PA, Eles JR, Lagenaur CF, Kozai TDY and Cui XT 2018 Unique electrophysiological and impedance signatures between encapsulation types: An analysis of biological Utah array failure and benefit of a biomimetic coating in a rat model Biomaterials 161 117–28 [PubMed: 29421549]

[51]. Branner A, Stein RB, Fernandez E, Aoyagi Y and Normann RA 2004 Long-Term Stimulation and Recording with a Penetrating Microelectrode Array in Cat Sciatic Nerve IEEE Trans. Biomed. Eng. 51 146–57 [PubMed: 14723504]

[52]. Thompson CH, Saxena A, Heelan N, Salatino J and Purcell EK 2021 Spatiotemporal patterns of gene expression around implanted silicon electrode arrays J. Neural Eng. 18

[53]. Thompson CH, Riggins TE, Patel PR, Chestek CA, Li W and Purcell E 2020 Toward guiding principles for the design of biologically-integrated electrodes for the central nervous system J. Neural Eng. 17

[54]. Hong G and Lieber CM 2019 Novel electrode technologies for neural recordings Nat. Rev. Neurosci. 20 330–45 [PubMed: 30833706]

[55]. Patel PR, Zhang H, Robbins MT, Nofar JB, Marshall SP, Kobylarek MJ, Kozai TDY, Kotov NA and Chestek CA 2016 Chronic in vivo stability assessment of carbon fiber microelectrode arrays J. Neural Eng. 13 1–15

[56]. Luan L, Wei X, Zhao Z, Siegel JJ, Potnis O, Tuppen CA, Lin S, Kazmi S, Fowler RA, Holloway S, Dunn AK, Chitwood RA and Xie C 2017 Ultraflexible nanoelectronic probes form reliable, glial scar–free neural integration Sci. Adv. 3

[57]. Yang X, Zhou T, Zwang TJ, Hong G, Zhao Y, Viveros RD, Fu TM, Gao T and Lieber CM 2019 Bioinspired neuron-like electronics Nat. Mater. 18 510–7 [PubMed: 30804509]

[58]. Obaid A, Wu Y-W, Hanna M, Jáidar O, Nix W, Ding J and Melosh N 2020 Ultra-sensitive measurement of brain penetration mechanics and blood vessel rupture with microscale probes bioRxiv 2020.09.21.306498

[59]. Stiller AM, Black BJ, Kung C, Ashok A, Cogan SF, Varner VD and Pancrazio JJ 2018 A meta-analysis of intracortical device stiffness and its correlation with histological outcomes Micromachines 9

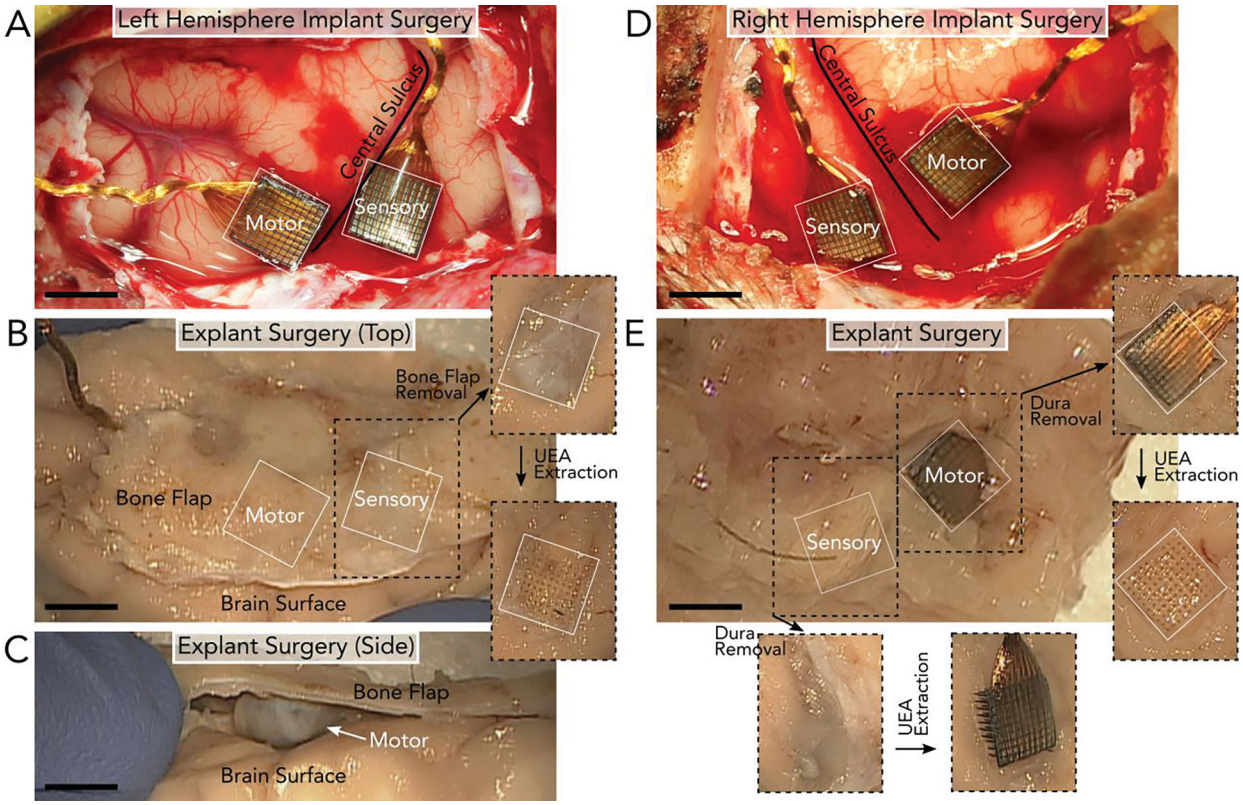

Figure 1.

Surgical implantation and explantation of UEAs after 848 days in the left hemisphere (A-C) and 590 days in the right hemisphere (D-E) of the NHP. A) Left hemisphere implantation of two UEAs in the motor and sensory cortices on either side of the central sulcus. B) Explantation of the UEAs in (A) involved removing the section of bone (bone flap) above the arrays. After the bone flap and dura were removed, the UEAs could be extracted. Removing the left sensory UEA revealed clear holes in the tissue. C) However, the UEA in the left motor cortex was fully encapsulated by tissue and no longer implanted in the brain surface, as seen from the image taken of the side of the tissue. Once removed, a depression in the brain surface was observed below the array's location. D) Right hemisphere implantation of two UEAs in the motor and sensory cortices on either side of the central sulcus. E) Explantation of the UEAs in (D) involved removing the bone flap above the arrays to reveal the two UEAs. After the bone flap was removed, the UEAs could be extracted. Both UEAs were partially or fully implanted in the tissue at the time of explant. Given the similarity between the landmarks surrounding the arrays during implantation (A & D) and explantation (B & E), we determined that the arrays largely retained their positions along the brain surface. All scale bars are 4mm.

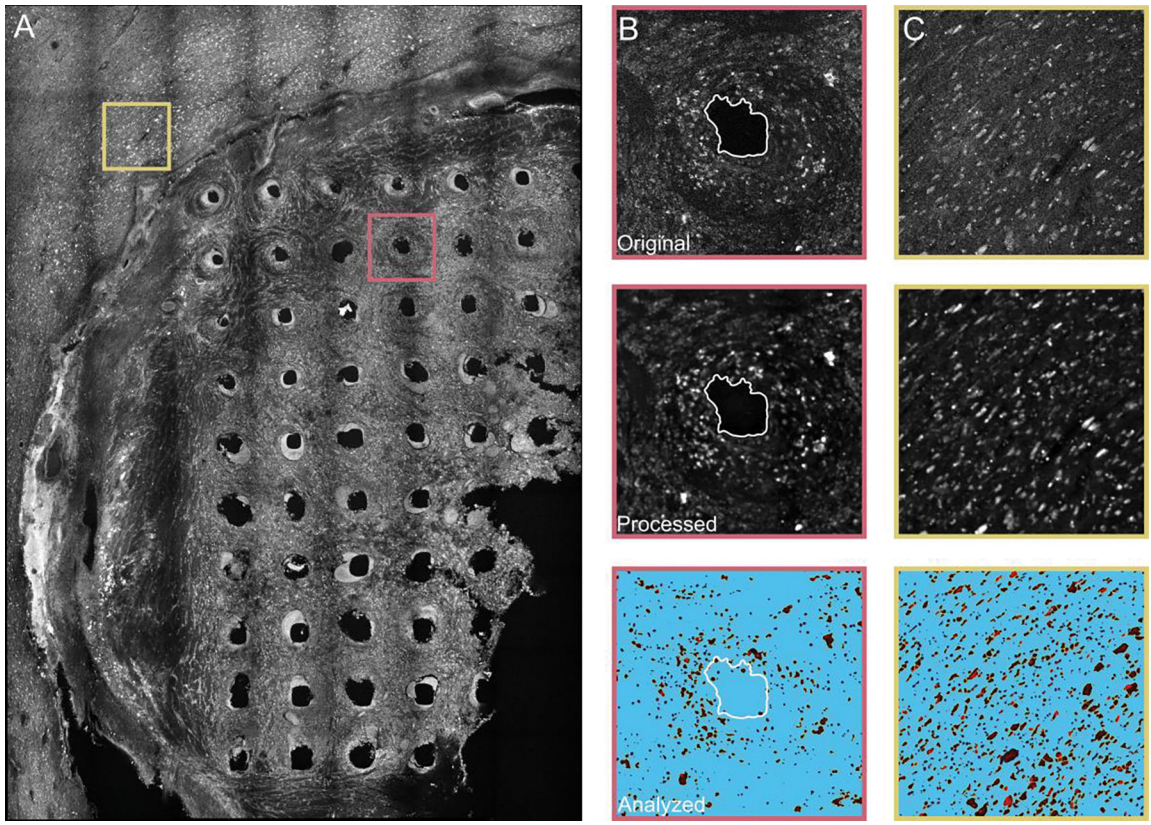

Figure 2.

Tissue analysis of NeuN staining of slice 11 in the left sensory cortex under the LS array. A) Confocal image of slice 11 (tissue 1000–1100 μm from brain surface) at a z-stack approximately in the center of the slice. Slice 11 shows 50 intact electrode shank holes and nearby non-implanted tissue. The pink box (400 μm × 400 μm) outlines a representative electrode shank hole seen in (B) and yellow box outlines the non-implanted tissue seen in (C). The representative electrode shank hole (B) and non-implanted tissue (C) are depicted in original form (top), after filtering and other processing steps (middle), and after analysis in ImageJ with the Analyze Particles program (bottom). Images in (B) and (C) are 400 μm × 400 μm.

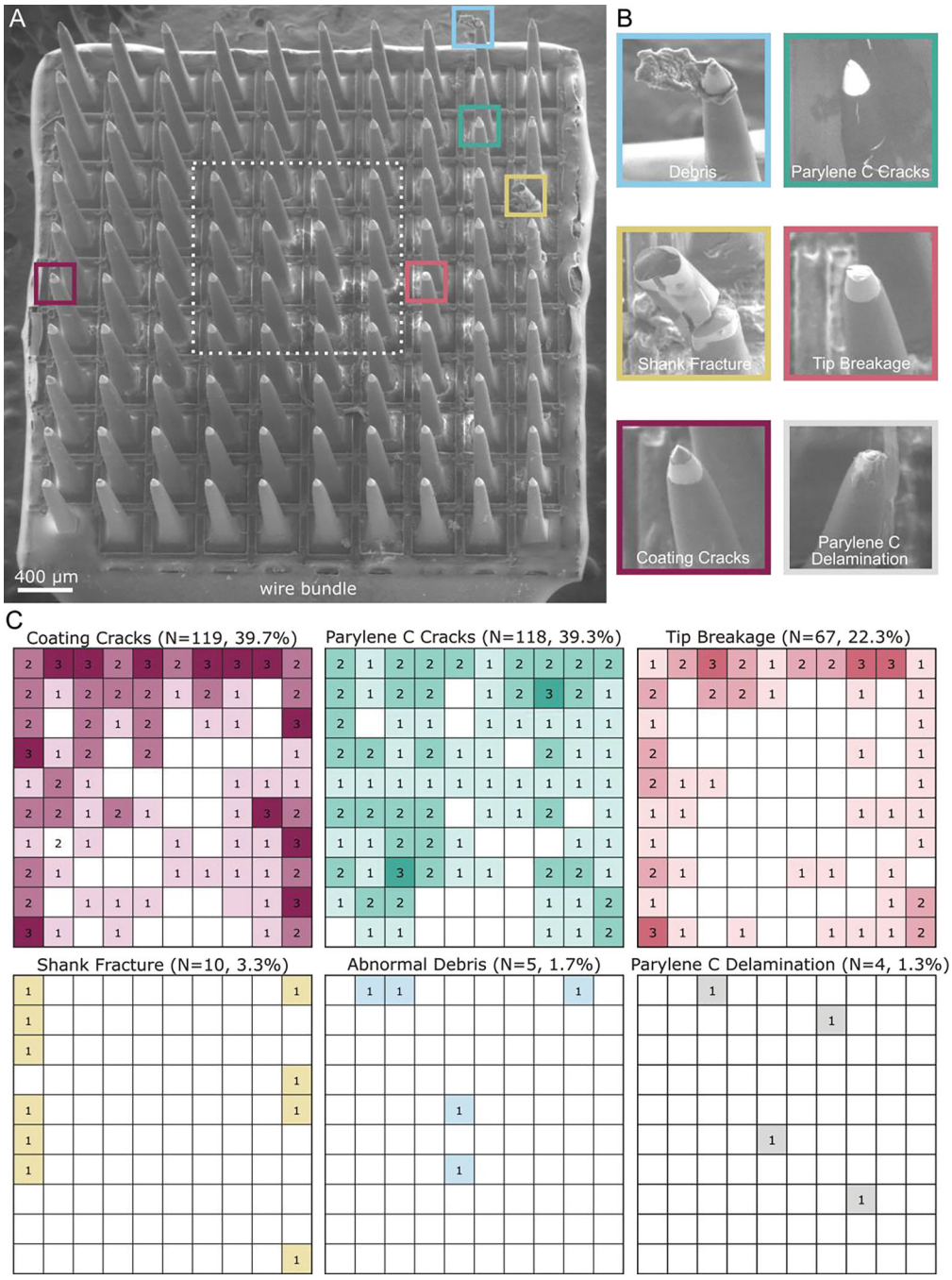

Figure 3.

Explanted UEA SEM images and analysis for degradation. A) SEM image of the UEA implanted in the left sensory cortex after 848 days. The UEA is oriented with the wire bundle on the bottom edge. B) Example images of the six categories quantified across three analyzed UEAs. Images of debris, Parylene C cracks, shank fracture, tip breakage, and coating cracks are from the UEA in the left sensory cortex in (A). The representative image of Parylene C delamination is from the UEA in the right motor cortex, as the UEA in the left sensory cortex did not exhibit Parylene C delamination. C) Heat maps of the summation

of categorical occurrences in the three analyzed UEAs. The orientation of each heat map is that of the image in (A). Coating cracks occurred most frequently (N=119 electrode shanks, 39.7%), followed by Parylene C cracks (N=118, 39.3%), and then tip breakage (N=67, 22.3%). Coating cracks and tip breakage were significantly more frequent in the outer three rows of electrode shanks than the inner four rows (p-value < 0.05). Shank fracture (N=10, 3.3%), abnormal debris (N=5, 1.7%), and Parylene C delamination (N=4, 1.3%) occurred less frequently.